Available online at www.sciencedirect.com

ScienceDirect

Energy Procedia 102 (2016) 87 – 95

Energy Procedia

E-MRS Spring Meeting 2016 Symposium T - Advanced materials and characterization techniques for solar cells III, 2-6 May 2016, Lille, France

Perovskite $FA_{1-x}MA_xPbI_3$ for solar cells: films formation and properties

B. Slimi[a,b,c], M. Mollar[a], I. Ben Assaker[b], I. Kriaa[d], R. Chtourou[b], B. Marí[a,*]

[a] *Institut de Disseny i Fabricació, Universitat Politècnica de València, Camí de Vera s/n, 46022 València, SPAIN*
[b] *Laboratoire Photovoltaïques, Centre de Recherches et des Technologies de l'Energie Technopole Borj Cedria, Bp 95, Hammam Lif 2050, Tunisie*
[c] *Faculté des Sciences de Bizerte, Université de Carthage, Tunisie*
[d] *Laboratoire de Chimie Moléculaire Organique, 5 Avenue Taha Houssein Monfleury, 1089 Tunis, Tunisie*

Abstract

Organic-inorganic hybrid perovskite formamidinium lead triiodide $NH_2CHNH_2PbI_3$ ($FAPbI_3$), methylammonium lead triiodide $CH_3NH_3PbI_3$ ($MAPbI_3$) and formamidinium methylammonium lead triiodide $(NH_2CHNH_2)_{1-x}(CH_3NH_2)_xPbI_3$ ($FA_{1-x}MA_xPbI_3$) thin films were synthesized and deposited on indium tin oxide glass substrates by spin coating process. Thin films of mixed $FA_{1-x}MA_xPbI_3$ (x = 0-1) perovskites obtained by mixing $FAPbI_3$ and $MAPbI_3$ in different proportions. The morphological, structural and optical proprieties of all synthetized perovskites have been analyzed as a function of the MA/FA ratio. X-ray diffraction analyses indicated the formation a cubic perovskite phase with space group Pm-3m in the composition range $0 \leq x \leq 1$. Mixed perovskites $FAMAPbI_3$ showed a high absorbance in the infrared region 780-900 nm. The band gap energy estimated from absorbance spectral measurements for $FAMAPbI_3$ thin films ranges from 1.50 eV for $FAPbI_3$ to 1.56 eV for $MAPbI_3$, respectively. The overall PL emissions of mixed FA/MA perovskite thin films are located in intermediate values between 773 nm and 810 nm.

Peer-review under responsibility of The European Materials Research Society (E-MRS).

Keywords: Organic-inorganic perovskites; Formamidinium Lead Iodide; planar heterojunction; Morphology control; Optical absorption; Photoluminescence.

* Corresponding author. Tel.: +34-963.877-5250; fax: +34-963-887-7189.
E-mail address: bmari@fis.upv.es

doi:10.1016/j.egypro.2016.11.322

1. Introduction

Hybrid organic-inorganic perovskite solar cells have become one of the most attractive photovoltaic technologies over the last five years due to their with simple synthesis from solution, high conversion efficiencies for devices and low costs fabrication [1-3]. First report on long-term durable 9.7% efficient perovskite solar cells based on methylammonium lead triiodide ($CH_3NH_3PbI_3$ or $MAPbI_3$) was released in 2012 [4] and the formamidinium lead triiodide ($HC(NH_2)_2PbI_3$ or $FAPbI_3$) perovskite, with broader light absorption delivering power conversion efficiency (PCE) up to 13.8% were reported in 2015 [5-9]. Subsequent improvements on the fabrication [10-12] and the annealing processes [13–15] and structure engineering for mixed perovskites [16-18] resulted in PCE higher than 15% [19-20]. Recently, perovskite solar cells have been classified as a new type of solar cell and a record PCE of 16.2% have been certified [21]. Perovskite solar cells have been selected as one of the biggest scientific breakthroughs of 2013 [22]. So far, the highest performance has overcome 20.1% [23].

Increasing the photocurrent by expanding the absorption spectra of ABX_3 perovskites by means of chemical modification has been proposed as a method for further improving solar cell efficiency. For example, replacing the methylammonium cation (MA^+) in $MAPbI_3$ with a formamidinium cation (FA^+), which has a larger ionic radius, results in an ABX_3 perovskite with a smaller bandgap for broader-spectrum light harvesting [24-26]. And the combining MAI with FAI in a sequential deposition method, the efficiencies of 14.9% and 16.01% were obtained [28-30]. In comparison to $MAPbI_3$, the more recently developed $FAPbI_3$ perovskite is less studied, despite the importance of efficiency in solar cells for example 16.6% [22]. The preparation of the high-quality black α-$FAPbI_3$ perovskite film is still a challenge, because the yellow δ-$FAPbI_3$ non-perovskite polymorph phase formed from one-step solution processing at room temperature is very hard to remove.

The crystal structure of $FAPbI_3$ is attributed to the larger ion size of FA^+ compared to MA^+ (the ionic radii of FA and MA are 2.79 and 2.70 Å, respectively [30]. Theoretically, the yellow δ-$FAPbI_3$ non-perovskite polymorph phase can transform to the photoactive black α-$FAPbI_3$ phase at high temperature (140 °C). Actually, it is not easy to fully transform δ-$FAPbI_3$ into α-$FAPbI_3$ when it fills the scaffold layer probably because of the stress from the substrate [31].

In this paper, we examine the effect of annealing temperature on the properties of mixed $FA_{1-x}MA_xPbI_3$ (x = 0-1) perovskites with different FA/MA ratios. Morphological, structural and optical properties of mixed $FA_{1-x}MA_xPbI_3$ perovskite films were studied as a function of their composition.

2. Experimental

2.1. Synthesis of Formamidinium Iodide [$HC(NH_2)_2I$] (FAI)

Formamidine iodide ($HC(NH_2)_2I$ or FAI) was synthesized by mixing 0.08 mol formamidine acetate (Sigma Aldrich) with 0.08 mol Hydriodic acid (HI) (57 wt. % in H_2O, distilled, stabilized, 99.95% from Sigma Aldrich). The mixture was stirred for 30 min in a round-bottom flask, which was kept in an ice bath (0 ºC). The solvent was then evaporated using a rotary evaporator and then the solid was recrystallized in ethanol two times. The solid obtained was washed thoroughly with ether until a white crystalline powder was obtained. The powders were finally dried under vacuum for one night before use. The elemental analysis shows the weight ratio of C:N:H in the as-prepared FAI is 7.30:16.46:2.83, which is in very good agreement with theoretical atomic ratio. It was found that the mixture of PbI_2 and FAI with a mole ratio of 1:1 was soluble in DMF.

Methylammonium iodide (CH_3NH_3I or MAI) from Sigma Aldrich was used as received.

2.2. Synthesis of thin film perovskites

$FAPbI_3$ and $MAPbI_3$ perovskites precursor solutions were prepared from an equimolar mixture of FAI/MAI and PbI_2 in dimethylformamide (DMF) solution at 40 %wt with ratios 1:1 (1:1 mol %) for FAI:PbI_2 and MAI:PbI_2 and then stirred for 2 h at 70 °C. The mixture was deposited on indium tin oxide (ITO) covered glass by spin-coating at 3500 rpm for 11 s. A drop of toluene was added after 2-4 s before the end then dried at 5000 rpm for 30 s. The

resulting perovskite layers were then annealed at 140 and 150 °C for 20 min. ITO glass substrates were previously cleaned with ethanol, isopropanol and water for 15 min respectively and then dried with clean dry air. Bulk $FAPbI_3$, $MAPbI_3$ and $FA_{1-x}MA_xPbI_3$ (x= 0-1) sample were prepared via drying DMF solution at different temperature on ITO substrates.

2.3. Characterization

Perovskite thin films were characterized by field-emission scanning electron microscopy (FE-SEM) (ZEISS UL TRA55) at an acceleration voltage of 10 kV, Energy Dispersive X-ray Spectrometer (EDX) mounted on the FE-SEM), X-ray diffraction is using a RIGAKU Ultima IV in the Bragg-Bentano configuration using *CuKα* radiation. Photoluminescence (PL) spectra were recorded at room temperature. The PL excitation source was a He-Cd laser at 325 nm. Photoluminescence data were recorded by a Si-based CCD detector Hamamatsu. Optical measurements were performed at room temperature using a spectrometer Ocean Optics HR4000 equipped with a Si-CCD detector. An integrating sphere was used to collect both direct and diffuse transmittance.

3. Results and discussion

3.1. X-ray analyses

Figure 1 shows the X-Ray diffractograms for $FAPbI_3$, $MAPbI_3$ and $FAMAPbI_3$ thin films. XRD peaks are located at 14.1, 20.0, 24.4, 28.4, 31.8, 40.6 and 43 degree for $MAPbI_3$ and slightly shifted to smaller angles for $FAPbI_3$. As an example the (0 0 1) peak is located at 13.8° for of α-$FAPbI_3$ and at 14.1° for $MAPbI_3$. The shift is due to the bigger size of FA cation with respect to MA cation that expands the crystal lattice. XRD peaks for composite $FA_{1-x}MA_xPbI_3$ perovskite films are located between those of $FAPbI_3$ and $MAPbI_3$ films and shift their position proportionally to the MA content. Such a gradual shift in diffraction peaks position angle indicates that mixed $FA_{1-x}MA_xPbI_3$ perovskite are formed with both organic cations (FA and MA) are inserted in the same lattice.

The yellow δ-phase of $FAPbI_3$ was produced at annealing temperatures below 150 °C, as indicated by the typical peak at 11.8° corresponding to non-perovskite structure. Increasing the annealing temperature to 170 °C the secondary phase (δ-$FAPbI_3$) disappears similarly for the mixed $FA_{1-x}MA_xPbI_3$ for x=0.2. The δ-$FAPbI_3$ phase in mixed perovskites disappears when the temperature increases and when FA content decreases, confirming that mixed FA/MA perovskites become more stable. The sharp diffraction peaks for the synthesized $MAPbI_3$, $FAPbI_3$ and $FA_{1-x}MA_xPbI_3$ films reveals the high crystallinity of the films. Further this fact is fairly consistent with the results found in literature [18].

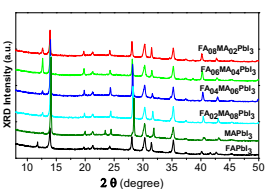

Figure 1. X-Ray diffractograms of the $FA_{1-x}MA_xPbI_3$ thin-films perovskites with different molar ratio of FA/MA (x= 0, 0.2, 0.4, 0.6, 0.8, 1).

Figure 2 shows a zoom in the region corresponding to (0 0 1) and (0 0 2) diffraction peaks. The position of the both peaks shifts to higher angles when the MA content in the thin film increases. (0 0 1) diffraction peaks are located at 13.915, 13.934, 13.966, 13.995, 14.025 and 14.106 degree for x = 0, 0.2, 0.4, 0.6, 0.8 and 1, respectively.

Diffraction peaks located at 21.26, 30.25, 35.16, 37.34 and 45.20 degree corresponding to ITO substrate is also observed. Since the XRD measurement system ensures an uncertainty for 2 θ lower than $\pm$ 0.02, the observed peak shifts are not due to experimental errors. The gradual diffraction angle shift indicates that the two cations are both inserted in the same lattice and the shift of peak maximum toward lower angle for increasing MA/FA ratios is indicative of an increase in lattice parameter. The changes in the lattice parameter are due to the incorporation of the larger FA^+ cation instead of the smaller organic MA^+ cation (the ionic radii of FA^+ and MA^+ are 2.79 and 2.70 Å, respectively) [32,33].

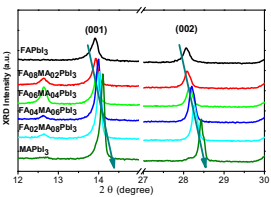

Figure 2. X-Ray diffractograms of the $FA_{1-x}MA_xPbI_3$ thin-films magnified view of the region 12–15° and 27-30°.

$FAPbI_3$ perovskite crystallizes in a cubic phase for temperatures higher than 150 °C. On the other hand, $MAPbI_3$ thin films crystallize and stabilize in a cubic phase Pm-3m at room temperature [34-38]. Mixed $FAMAPbI_3$ perovskites crystallize in the same cubic structure corresponding to the spatial group labeled as P432 (Pm-3m). The lattice parameters of $FAPbI_3$ are calculated to be a=6.352 Å, which is in good agreement with previously reported phase for $FAPbI_3$ [39, 28].

Table 1: Lattice parameters of mixed $FA_{1-x}MA_xPbI_3$ perovskite films as a function of MAI composition (x), when x varies in the range 0-1.

MAI concentration (x) in $FAI_{1-x}MAI_xPbI_3$	0	0.2	0.4	0.6	0.8	1
a (Å)	6.352	6.346	6.339	6.323	6.309	6.270

The lattice parameters of mixed $FA_{1-x}MA_xPbI_3$ thin film perovskites are shown in Table 1. The lattice parameters of $MAPbI_3$ are calculated to be a = 6.270 and the $FAPbI_3$ a=6.352 Å, exhibits the lattice parameter (a) of the $FA_{1-x}MA_xPbI_3$ phases indexed by cubic as a function of MA content (x). The lattice parameters increase with the decrease of MA content. Despite of the phase of $FAPbI_3$, the lattice parameter of $FA_{1-x}MA_xPbI_3$ ($0 \leq x \geq 1$) phases exhibits a linear relationship with the FA content in each region. Therefore, the linear trend indicates the formation of the $FA_{1-x}MA_xPbI_3$ with change of lattice parameters rather than phase of $MAPbI_3$.

3.2. SEM and EDX analyses

FE-SEM studies were conducted to examine the influence of MA incorporation in the morphology of thin films. Figure 3 presents' top views FE-SEM images of the $FAPbI_3$, $MAPbI_3$ and $FA_{1-x}MA_xPbI_3$ perovskite thin films deposited on ITO substrates with different MA fractions. The $FA_{1-x}MA_xPbI_3$ film has a dense and a homogenous morphology with fiber-like crystals with the presence of void due to solvent evaporation and some crevices between

the crystal boundaries. In case of $FA_{1-x}MA_xPbI_3$, it consists of aggregate crystals with some cracks. The obtained films with different MA content have a different shape, morphology and size. Indeed, as the composition x increases, the aggregation of gains decreased, due to the volume between the two cations of FA and MA.

The disappearance of the yellow δ-$FAPbI_3$ phase can also be monitored via the SEM micrographs. Here the needle-like crystals obtained for low MA contents can be correlated to the existence of δ-$FAPbI_3$ phase. Needle-like morphologies (low MA contents) are connected with the disappearance of XRD reflections corresponding to the cubic structure. Higher amounts of MA result in the stabilization of the α-$FAPbI_3$ phase.

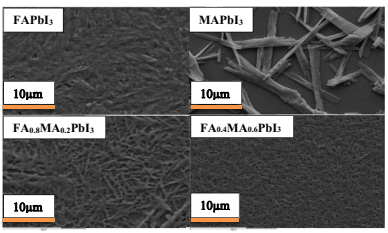

Fig 3. FESEM images of $FA_{1-x}MA_xPbI_3$ thin films arrays grown over large surface areas on ITO substrates.

Table 2 displays the EDX results of all synthesized samples. FA, MA, Pb and I elements are homogeneously distributed in the crystals perovskite, suggesting that Pb and I are uniformly incorporated in the $FAPbI_3$, $MAPbI_3$ and $FA_{1-x}MA_xPbI_3$ in grain perovskite rather than existing in separate chemical phases. The results analysis of EDX for all films shows that the between Pb and I are very close to the theoretical values, which are 75% and ≈25% for I and Pb, respectively.

Table 2: EDX analysis for Iodine and Lead content in mixed $FA_{1-x}MA_xPbI_3$ thin films (x=0-1).

Perovskites	Pb (Atomic %)	I (Atomic %)
$FAPbI_3$	24.25	75.75
$FA0.8MA0.2PbI_3$	24.09	75.91
$FA0.6MA0.4PbI_3$	23.97	76.03
$FA0.4MA0.6PbI_3$	23.59	76.41
$FA0.2MA0.8PbI$	23.31	76.69
$MAPbI_3$	23.84	76.16

3.3. UV–vis spectra

The absorption spectra of $FA_{1-x}MA_xPbI_3$ thin films on ITO are presented in Figure 4. The trend is lower the MA content the lower the cutoff wavelength. The $MAPbI_3$ exhibits the lowest cutoff wavelength while $FAPbI_3$ has the highest and cutoff wavelengths for mixed $FA_{1-x}MA_xPbI_3$ are between. A systematic shift of the absorption band edge to longer wavelengths when the MA content increases is observed. Therefore perovskite band gap can be tuned by varying MA percentage in the loading solution.

The onset of bandgap absorption for $FAPbI_3$ and $MAPbI_3$ thin films is around 825 nm, 793nm (corresponding to energy of 1.50 and 1.56 eV, respectively) is similar to previous observation [26]. The narrower band gap of $FAPbI_3$ makes it feasible to absorb light over ≈800 nm and switches a greater inverse proportion of the sun energy to electricity.

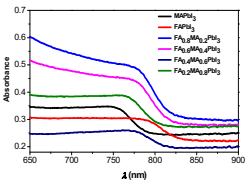

Figure 4. The UV-visible absorption spectra from 650 nm to 900 nm for $FA_{1-x}MA_xPbI_3$ (x = 0-1) thin films.

Figure 5 shows the evolution of the interplanar spacing depending on percentage of MA, decrease in the amount of MA distance increases is well explains the effect of the cation size so it confirms both cations are well mixed. As the MA content increases, the absorbance edge shifts to short wavelength values, indicating the increase of the band gap energy of the prepared perovskite thin films. The onset band gap of mixed $FA_{1-x}MA_xPbI_3$ perovskite thin films are located in intermediate values between 1.563 eV ($MAPbI_3$) and 1.502 eV ($FAPbI_3$) meaning that the band gap can be tuned by varying the composition of the ratio FA/MA (See Table 3)[4-6]. The results are in good agreement with theory, which predicts that the higher the content of MA cation the higher the band gap energy. In addition band gap energy for mixed $FA_{1-x}MA_xPbI_3$ perovskites is between the band gap energies of $MAPbI_3$ and $FAPbI_3$ which further support this claim a new phase synthesized. It is also worthy to notice that for absorption measurements we used an integrating sphere to collect the direct and diffuse transmittance in order to remove the effect of light scattering originating from refraction and reflection phenomenon inside the perovskite crystals.

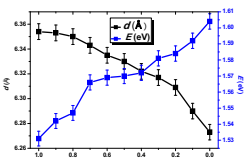

Figure 5. Interplanar spacing (d) and band gap energy (Eg) as a function of [FA/MA] ratio.

3.4. Luminescence properties

Figure 6 shows the normalized PL spectra of the mixed $FA_{1-x}MA_xPbI_3$ thin films. A significant red shift (about 37 nm) in the emission peak from $MAPbI_3$ (λmax=773 nm) to $FAPbI_3$ (λmax=810 nm) was observed consistent with the absorption spectrum along with a noticeable broadening of the emission profile [40]. The gradual shift in emission indicates the formation of a solid solution of FA/MA in the perovskite lattice. Here, we also observe a gradual transition from $MAPbI_3$ to $FAPbI_3$ in PL spectra, in good agreement with the XRD and absorbance spectra again indicating that the transition between perovskites occurs via fully crystalline mixed cation phases. The similarity of the observed trends suggests that the ratio of intercalated cations is similar to that of the dissolved cations in the precursor solution. The nonlinearity of the emission shift reflects interactions between FA and MA cations.

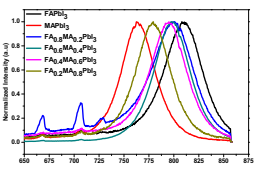

Fig 5. Normalized PL at room temperature for mixed $FA_{1-x}MA_xPbI_3$ (x = 0, 0.2, 0.4, 0.6, 0.8, 1) perovskite thin films.

Table 3 shows the energy position of the absorption edge and the position of the PL peak at room temperature for the mixed perovskite $FA_{1-x}MA_xPbI_3$ (x=0-1) thin films synthesized in this work. The wavelength position of the maximum of emission is shifted to lower wavelengths when compared with the onset of the absorption edge of $FAPbI_3$ (810 nm) up to $MAPbI_3$ (773 nm). The component of PL spectra with the highest energy corresponds to transitions from the conduction band to the valence band and the lower energy components of the PL spectra involve energy levels inside the band gap, which is in agreement with the sub band gap absorption mentioned before. The wavelength position of the maximum of the photoluminescence emission is shifted to the lowest wavelengths when compared with the inset of the absorption edge, but with a small displacement related to the concentration of MA.

The high intensity of PL emission suggests that most decay transitions are radiative and nonradiative decay is negligible. Since the radiative recombination dominates one can speculate that most energy levels inside the band gap correspond to shallow levels and electron-hole pairs formed during optical excitation recombine radiatively emitting photons. The amount of deep levels inside the bandgap is very low and as a result both pure and mixed perovskites exhibit high luminescent efficiency.

Table 3: The estimated band gap for the PL and absorption with the variation of FA/MA ratio.

Perovskites	*Eg* (Abs) (eV)	*Eg* (PL) (eV)
$FAPbI_3$	1.502	1.531
$FA_{0.8}MA_{0.2}PbI_3$	1.507	1.547
$FA_{0.6}MA_{0.4}PbI_3$	1.514	1.569
$FA_{0.4}MA_{0.6}PbI_3$	1.530	1.572
$FA_{0.2}MA_{0.8}PbI_3$	1.554	1.584
$MAPbI_3$	1.563	1.604

4. Conclusion

The mixed $FA_{1-x}MA_xPbI_3$ perovskites prepared by mixing $FAPbI_3$ and $MAPbI_3$ in the desired proportions (x=0-1), were synthetized and deposited as thin films onto ITO substrates by spin coating in one step. All synthetized $FA_{1-x}MA_xPbI_3$ (x=0-1) perovskites reported in this paper crystallized in the same cubic phase irrespective of the x the value and a unique spatial group Pm-3m (P432) was observed. The evolution of the angle 2θ and increases for all samples and directly related to the increase in MA. Absorbance measurement shows that the perovskite films exhibit a very high absorbance in the infrared region. The absorption edge of the thin films can be tuned along the visible spectrum from 650 nm to 900 nm. The band gap energy of perovskite thin film was estimated from absorbance spectral measurement, it was found that the onset of the absorption edge for $FA_{1-x}MA_xPbI_3$ thin films reaching intermediate values ranges from 1.50 ($FAPbI_3$) to 1.56 eV ($MAPbI_3$). In the PL study, the incorporation of MA into $FAMAPbI_3$ shifts the PL emission to shorter wavelengths, the overall PL emission of mixed FA/MA perovskite thin films are located in intermediate values between 810 nm ($FAPbI_3$) and 773 nm ($MAPbI_3$). Finally the results obtained confirmed that the mixed perovskites were synthesized.

Acknowledgements

This work was supported by Ministerio de Economía y Competitividad (ENE2013-46624-C4-4-R) and Generalitat valenciana (Prometeus 2014/044).

References

[1] Gratzel M. The light and shade of perovskite solar cells. Nat Mater 2014:13:838-842.
[2] Jeon NJ, Noh JH, Kim YC, Yang WS, Ryu S, Seok SI. Solvent engineering for high-performance inorganic–organic hybrid perovskite solar cells. Nat Mater 2014:13:897–903.
[3] Jeon NJ, Noh JH, Yang WS, Kim YC, Ryu S, Seo J, Seok SI. Compositional engineering of perovskite materials for high-performance solar cells. Nature 2015:517:476-480.
[4] Kim HS, Lee CR, Im JH, Lee KB, Moehl T, Marchioro A, Moon SJ, Humphry-Baker R, Yum JH, Moser JE, Grätzel M, Park NG. Lead Iodide Perovskite Sensitized All-Solid-State Submicron thin Film Mesoscopic Solar Cell with Efficiency Exceeding 9%. Sci Rep 2012:2:591.
[5] Zhou Y, Yang M, Vasiliev AL, Garces HF, Zhao Y, Wang D, Pang S, Zhu K, Padture NP. Growth Control of Compact $CH_3NH_3PbI_3$ thin Films via Enhanced Solid-State Precursor Reaction for Efficient Planar Perovskite Solar Cells. J Mat Chem A 2015:3:9249-9256.
[6] Jeon NJ, Noh JH, Yang WS, Kim YC, Ryu S, Seo J and Seok SI. Compositional engineering of perovskite materials for high-performance solar cells. Nature 2015:517:476.
[7] Eperon GE, Stranks SD, Menelaou C, Johnston MB, Herz LM and Snaith HJ. Formamidinium lead trihalide: a broadly tunable perovskite for efficient planar heterojunction solar cells. Energy Environ Sci 2014:7:982-988.
[8] Lv S, Pang S, Zhou Y, Padture NP, Hu H, Wang L, Zhou X, Zhu H, Zhang L, Huang C and Cui G. One-step, solution-processed formamidinium lead trihalide ($FAPbI_{3-x}Cl_x$) for mesoscopic perovskite–polymer solar cells. Phys Chem Chem Phys 2014:16:19206.
[9] Zhu K, Miyasaka T, Kim JK and Mora-Seró I. Trend of Perovskite Solar Cells: Dig Deeper to Build Higher. J Phys Chem Lett 2015:6:2315.
[10] Burschka J, Pellet N, Moon SJ, Humphry-Baker R, Gao P, Nazeeruddin MK and Gratzel M. Sequential deposition as a route to high-performance perovskite-sensitized solar cells. Nature 2013:499:316.
[11] Xiao M, Huang F, Huang W, Dkhissi Y, Zhu Y, Etheridge J, Gray-Weale A, Bach U, Cheng YB and Spiccia L. A Fast Deposition-Crystallization Procedure for Highly Efficient Lead Iodide Perovskite Thin-Film Solar Cells. Angew Chem Int Ed 2014:126:10056.
[12] Nie W, Tsai H, Asadpour R, Blancon JC, Neukirch AJ, Gupta G, Crochet JJ, Chhowalla M, Tretiak S, Alam MA, Wang HL and Mohite AD. High-efficiency solution-processed perovskite solar cells with millimeter-scale grains. Science 2015:347:522-525.
[13] Eperon GE, Burlakov VM, Docampo P, Goriely A and Snaith HJ. Morphological Control for High Performance, Solution Processed Planar Heterojunction Perovskite Solar Cells. Adv Funct Mater 2014:24:151.
[14] Kang R, Kim JE, Yeo JS, Lee S, Jeon YJ and Kim DY, Optimized Organometal Halide Perovskite Planar Hybrid Solar Cells via Control of Solvent Evaporation Rate. J Phys Chem C 2014:118:26513.
[15] Xie FX, Zhang D, Su H, Ren X, Wong KS, Gratzel M and Choy WCH. Vacuum-A ssisted Thermal Annealing of CH3NH3PbI3 for Highly Stable and Efficient Perovskite Solar Cells. ACS Nano 2015:9:639.
[16] Lee MM, Teuscher J, Miyasaka T, Murakami TN and Snaith HJ. Efficient Hybrid Solar Cells Based on Meso-Superstructured Organometal Halide Perovskites. Science 2012:338:643.
[17] Liu M, Johnston MB and Snaith HJ. Efficient planar heterojunction perovskite solar cells by vapour deposition. Nature 2013:501:395.
[18] Malinkiewicz O, Yella A, Lee YH, Espallargas GM, Graetzel M, Nazeeruddin MK and Bolink HJ. Perovskite solar cells employing organic charge-transport layers. Nat Photonics 2014:8:128.

[19] Kojima A, Teshima K, Shirai Y and Miyasaka T. Organometal Halide Perovskites as Visible-Light Sensitizers for Photovoltaic Cells. J Am Chem Soc 2009:131:6050-6051.
[20] Lee JW, Seol DJ, Cho AN, Park NG. High-efficiency perovskite solar cells based on the black polymorph of $HC(NH_2)_2PbI_3$. Adv Mater 2014: 26:4991-4998.
[21] Wozny S, Yang M, Nardes AM, Mercado CC, Ferrere S, Reese MO, Zhou W and Zhu K. Controlled Humidity Study on the Formation of Higher Efficiency Formamidinium Lead Triiodide-Based Solar Cells. Chem Mater 2015:27:4814-4820.
[22] Science News. Breakthrough of the Year. Newcomer Juices Up the Race to Harness Sunlight. Science 2013:342:1438.
[23] Yang WS, Noh JH, Jeon NJ, Kim YC, Ryu S, Seo J, Seok SI. High-performance photovoltaic perovskite layers fabricated through intramolecular Exchange. Science 2015:348:1234.
[24] Zhou Y, Yang M, Kwun J, Game OS, Zhao Y, Pang S, Padture NP, Zhu K. Intercalation crystallization of phase-pure α- $HC(NH_2)_2PbI_3$ upon microstructurally engineered PbI_2 thin films for planar perovskite solar cells Nanoscale. 2016:8:6265-6270.
[25] Binek A, Hanusch FC, Docampo P, Bein T. Stabilization of the Trigonal High-Temperature Phase of Formamidinium Lead Iodide. J Phys Chem Lett 2015:6:1249 .
[26] Jeon NJ, Noh JH, Yang WS, Kim YC, Ryu S, Seo J, Seok SI. Compositional engineering of perovskite materials for high-performance solar cells. Nature 2015:517: 476.
[27] Pang S, Hu H, Zhang J, Lv S, Yu Y, Wei F, Qin T, Xu H, Liu Z and Cui G. $NH_2CH{=}NH_2PbI_3$: An Alternative Organolead Iodide Perovskite Sensitizer for Mesoscopic Solar Cells. Chem Mater 2014:26:1485–1491.
[28] Eperon G, Stranks S, Menelaou C, Johnston M, Herz L and Snaith H, Formamidinium lead trihalide: a broadly tunable perovskite for effi cient planar heterojunction solar cells. Energy Environ Sci 2014:7:982-988.
[29] Pellet N, Gao P, Gregori G, Yang TY, Nazeeruddin MK, Maier J and Gratzel M, Mixed-Organic-Cation Perovskite Photovoltaics for Enhanced SolarLight Harvesting. Angew Chem Int Ed 2014:53:3151-3157.
[30] Koh TM, Fu K, Fang Y, Chen S, Sum TC, Mathews N, Mhaisalkar SG, Boix PP, and Baikie T. Formamidinium-Containing Metal-Halide: An Alternative Material for Near-IR Absorption Perovskite Solar Cells. J Phys Chem C :2014:118:16458-16462.
[31] Wang Z, Zhou Y, Pang S, Xiao Z, Zhang J, Chai W, Xu H, Liu Z, Padture NP and Cui G. Additive-Modulated Evolution of $HC(NH_2)_2PbI_3$ Black Polymorph for Mesoscopic Perovskite Solar Cells. Chem Mater 2015:27:7149–7155.
[32] Lee JW, Kim DH, Kim HS, Seo SW, Cho SM, Park NG. Formamidinium and Cesium Hybridization for Photo- and Moisture-Stable Perovskite Solar Cell. Adv Energy Mater 2015:5:1501310.
[33] Yuan DX, Gorka A, Xu MF, Wang ZK, Liao LS. Inverted planar $NH_2CH{=}NH_2PbI_3$ perovskite solar cells with 13.56% efficiency via low temperature processing. Phys Chem Chem Phys 2015:17: 19745-19750.
[34] Weller MT, Weber OJ, Frost JM, Walsh AJ. Cubic Perovskite Structure of Black Formamidinium Lead Iodide, α-$[HC(NH_2)_2]PbI_3$, at 298 K. Phys Chem Lett 2015:6:3209-3212
[35] Vega E, Mollar M and Marí B. Synthesis of $MAPbBr_{3-Y}I_Y$ (Y=I, Cl and i=0, 1, 2, 3) thin film perovskites. Physica Status Solidi C 2015:1-5
[36] Ong KP, Goh TW, Xu Q and Huan A. Structural Evolution in Methylammonium Lead Iodide $CH_3NH_3PbI_3$. J Phys Chem A 2015:119: 11033-11038.
[37] Huang W, Manser JS, Kamat PV and Ptasinska S. Evolution of Chemical Composition, Morphology, and Photovoltaic Efficiency of $CH_3NH_3PbI_3$ Perovskite under Ambient Conditions Chem Mater 2016:28:303-311.
[38] Gottesman R, Haltzi E, Gouda L, Tirosh S, Bouhadana Y and Zaban A. Extremely Slow Photoconductivity Response of $CH_3NH_3PbI_3$ Perovskites Suggesting Structural Changes under Working Conditions. J Phys Chem Lett 2014:5:2662-2669.
[39] Weller MT, Weber OJ, Henry PF, Di Pumpo AM, Hansen TC. Complete structure and cation orientation in the perovskite photovoltaic methylammonium lead iodide between 100 and 352 K. Chem Commun 2015:51: 4180-4183.
[40] T. Koh, K. Fu, Y. Fang, S. Chen, T. Sum, N. Mathews, S. Mhaisalkar, P. Boix and T. Baikie, J. Formamidinium-Containing Metal Halide: An Alternative Material for Near-IR Absorption Perovskite Solar Cells. Phys. Chem. C, 2014, 118, 16458-16462.